12. Yu. A. Surkov *et al.*, *Kos. Issled.* **14**, 704 (1976).
13. Yu. A. Surkov *et al.*, *Proc. Lunar Sci. Conf.* **8**, 2665 (1977).
14. O. V. Nikolaeva, *Earth Moon Planets* **50/51**, 329 (1990).
15. J. W. Head and L. Wilson, *J. Geophys. Res.* **91**, 3049 (1986).
16. P. C. Hess and J. W. Head, *Earth Moon Planets* **50/51**, 57 (1990).
17. C. Sotin, D. A. Senske, J. W. Head, E. M. Parmentier, *Earth Planet. Sci. Lett.* **95**, 321 (1989).
18. D. R. Williams and V. Pan, *Geophys. Res. Lett.* **17**, 1397 (1990).
19. G. H. Pettengill *et al.*, *Science* **252, 260** (1991).
20. G. L. Tyler *et al.*, *ibid.*, p. 265.
21. E. N. Slyuta *et al.*, *Astron. Vestn.* **22**, 287 (1988).
22. J. B. Garvin and R. S. Williams, *Geophys. Res. Lett.* **17**, 1381 (1990).
23. D. L. Swanson *et al.*, *U.S. Geol. Surv. Prof. Pap.* **1056**, 1 (1979).
24. R. Greeley, *J. Geophys. Res.* **87**, 2705 (1982).
25. M. H. Carr, *Icarus* **22**, 1 (1974); G. Hulme, *Mod. Geol.* **4**, 107 (1973).
26. J. W. Head and L. Wilson, *Lunar Planet. Sci.* **XI**, 426 (1980).
27. R. Greeley, *Science* **172**, 722 (1971).
28. E. N. Slyuta and M. A. Kreslavsky, *Lunar Planet. Sci.* **XXI**, 1174 (1990).
29. D. A. Senske, *Earth Moon Planets* **50/51**, 305 (1990).
30. E. N. Slyuta, *Lunar Planet. Sci.* **XXI**, 1172 (1990).
31. G. G. Schaber and R. C. Kozak, *U.S. Geol. Surv. Open File Rep.* **90-24** (1990).
32. D. A. Senske *et al.*, *Earth Moon Planets*, in press.
33. B. A. Campbell and D. B. Campbell, *Geophys. Res. Lett.* **17**, 1353 (1990).
34. L. Wilson, J. W. Head, and D. B. Campbell, *Lunar Planet. Sci.* **XXI**, 1347 (1990).
35. H. Sigurdsson and R. S. J. Sparks, *Nature* **274**, 126 (1978).
36. A. A. Pronin, *Geotectonics* **20**, 271 (1986).
37. K. M. Roberts and J. W. Head, *Earth Moon Planets* **50/51**, 193 (1990).
38. L. Wilson and J. W. Head, *Lunar Planet. Sci.* **XXI**, 1343 (1990).
39. C. Elachi *et al.*, *IEEE Trans. Geosci. Rem. Sens.* **GE22**, 383 (1984).
40. J. E. Guest and J. Sanchez, *Bull. Volcanol.* **33**, 778 (1969); B. Bonnichsen and D. F. Kaufman, *Geol. Soc. Am. Spec. Pap.* **212**, 119 (1987).
41. J. H. Fink and Manley (1987) *Geol. Soc. Am. Spec. Pap.* **212**, 77 (1987).
42. D. L. Swanson and R. T. Holcomb, in *Lava Flows and Domes*, J. H. Fink, Ed. (Springer-Verlag, Berlin, 1990), pp. 3–24.
43. R. M. Iverson, in *ibid.*, pp. 47–69.
44. S. Blake, in *ibid.*, pp. 88–126.
45. J. H. Fink, M. C. Malin, S. W. Anderson, *Nature* **348**, 435 (1990).
46. H. Williams, *Bull. Dept. Geol. Sci. Univ. Calif.* **21**, 51 (1932).
47. J. H. Fink, Ed. *Geol. Soc. Am. Spec. Pap.* **212** (1987).
47a. A. T. Basilevsky, personal communication.
48. J. A. Crisp, *J. Volcanol. Geotherm. Res.* **20**, 177 (1984).
49. A. Knopf, *Geol. Soc. Am. Bull.* **47**, 1727 (1936).
50. K. Nakamura, *J. Volcanol. Geotherm. Res.* **2**, 1 (1977).
51. G. G. Schaber, C. Elachi, T. G. Farr, *Remote Sens. Environ.* **9**, 149 (1980).
52. J. A. Crisp and S. Baloga, *Icarus* **85**, 512 (1990).
53. L. Wilson and J. W. Head, *Lunar Planet. Sci.* **XI**, 1260 (1980).
54. H. Huppert *et al.*, *Nature* **309**, 19 (1984).
55. R. S. Saunders *et al.*, *Science* **252, 249** (1991).
56. J. W. Head, *Earth Moon Planets* **50/51**, 5 (1990).
57. S. C. Solomon *et al.*, *Science* **252**, 297 (1991).
58. D. B. Campbell *et al.*, *ibid.* **251**, 181 (1991).
59. D. A. Senske *et al.*, *Earth Moon Planets*, in press.
60. V. P. Kryuchkov and A. T. Basilevsky, *Lunar Planet. Sci.* **XX**, 548 (1989).
61. T. L. Tolan *et al.*, *Geol. Soc. Am. Spec. Pap.* **239**, 1 (1989).
62. V. L. Barsukov *et al.*, *Geochimica* **12**, 1811 (1984).
63. E. R. Stofan and J. W. Head, *Icarus* **83**, 216 (1990).
64. A. A. Pronin and E. R. Stofan, *ibid.* **87**, 452 (1990).
65. D. A. Senske *et al.*, *Lunar Planet. Sci.* **XXI**, 1128 (1990).
66. J. W. Head, *Geology* **18**, 99 (1990).
67. _____ and J. D. Burt, *Lunar Planet. Sci.* **XXI**, 481 (1990).
68. V. P. Kryuchkov, *Earth Moon Planets* **50/51**, 471 (1990).
69. S. L. Frank and J. W. Head, *ibid.*, p. 421.
70. A. L. Sukhanov and A. A. Pronin, *Proc. Lunar Planet. Sci. Conf.* **19**, 335 (1989).
71. L. S. Crumpler *et al.*, *Geology* **14**, 1031 (1986).
72. K. M. Roberts and J. W. Head, *Geophys. Res. Lett.* **17**, 1341 (1990).
73. L. Wilson, J. W. Head, E. A. Parfitt, *Vernadsky/Brown Microsymp. 12* **2**, 37 (1990).
74. R. J. Phillips *et al.*, *Science* **252, 288** (1991).
75. A. L. Sukhanov *et al.*, *Astron. Vestn.* **21**, 195 (1987).
76. D. L. Bindschadler and J. W. Head, *J. Geophys. Res.*, in press.
77. S. C. Solomon and J. W. Head, *Science* **252**, 252 (1991).
78. S. R. Taylor, *Tectonophysics* **161**, 147 (1989).
79. R. White and D. McKenzie, *J. Geophys. Res.* **94**, 7685 (1989).
80. R. E. Grimm and S. C. Solomon, *Geophys. Res. Lett.* **14**, 538 (1987).
81. Quetzalpetlatl Corona and Mylitta Fluctus have been proposed as names to the IAU, but as of this writing the names have not been officially approved.
82. Unpublished maps by A. T. Basilversky (personal communication) aided our interpretation.
83. We gratefully acknowledge the Magellan Team at JPL, Martin-Marietta, and Hughes for their dedication to obtaining the data. D. Senske prepared the maps of Sif Mons and contributed to the discussion of Western Eistla Regio. K. Roberts prepared the maps of Sacajawea Patera and contributed to the discussion of Sacajawea and Mylitta Fluctus. J. Aubele and E. Slyuta prepared maps of the small shields and contributed to the discussion. B. Klose and B. Pavri contributed to the discussion of the steep-sided domes. D. Bindschadler and E. Stofan contributed to the discussion of the coronae. S. Keddie contributed to the discussion of cryptodomes. P. Fisher, E. Grosfils, A. deCharon, M. Bulmer, A. T. Basilevsky, V. Kryuchkov, and T. Parker contributed to the discussion and review of this paper. Special thanks to S. Yewell, J. Clark, J. Clough, and R. Post for preparation of images and figures. We gratefully acknowledge helpful reviews from J. Garvin and an anonymous reviewer.

22 January 1991; accepted 20 March 1991

Impact Craters on Venus: Initial Analysis from Magellan

ROGER J. PHILLIPS, RAYMOND E. ARVIDSON, JOSEPH M. BOYCE, DONALD B. CAMPBELL, JOHN E. GUEST, GERALD G. SCHABER, LAURENCE A. SODERBLOM

Magellan radar images of 15 percent of the planet show 135 craters of probable impact origin. Craters more than 15 km across tend to contain central peaks, multiple central peaks, and peak rings. Many craters smaller than 15 km exhibit multiple floors or appear in clusters; these phenomena are attributed to atmospheric breakup of incoming meteoroids. Additionally, the atmosphere appears to have prevented the formation of primary impact craters smaller than about 3 km and produced a deficiency in the number of craters smaller than about 25 km across. Ejecta is found at greater distances than that predicted by simple ballistic emplacement, and the distal ends of some ejecta deposits are lobate. These characteristics may represent surface flows of material initially entrained in the atmosphere. Many craters are surrounded by zones of low radar albedo whose origin may have been deformation of the surface by the shock or pressure wave associated with the incoming meteoroid. Craters are absent from several large areas such as a 5 million square kilometer region around Sappho Patera, where the most likely explanation for the dearth of craters is volcanic resurfacing. There is apparently a spectrum of surface ages on Venus ranging approximately from 0 to 800 million years, and therefore Venus must be a geologically active planet.

IMPACT CRATERS ON VENUS PROVIDE new information on the physics of cratering processes, including interaction with the atmosphere during meteoroid transit and atmospheric effects on cratering mechanics and ejecta formation. The modification of impact craters yields information on surface and interior processes, particularly tectonism and volcanism. The geographical distribution and abundance of craters provide constraints on the rate of resurfacing of the planet and, thus, the level of geological activity over the last several hundred million years.

After 37 days of operation, or 277 orbits covering approximately 56° of longitude, a total of 135 craters ranging from 3 to 105 km in diameter have been interpreted as having a high probability of impact origin. They lie within an area of 70×10^6 km^2, or about 15% of the planet's surface. If the area

R. J. Phillips, Department of Geological Sciences, Southern Methodist University, Dallas, TX 75275.
R. E. Arvidson, McDonnell Center for the Space Sciences, Department of Earth and Planetary Sciences, Washington University, St. Louis, MO 63130.
J. M. Boyce, Solar System Exploration Division, National Aeronautics and Space Administration, Washington, DC 20546.
D. B. Campbell, Department of Astronomy, Cornell University, Ithaca, NY 14853.
J. E. Guest, University of London Observatory, London, NW7 2QS England.
G. G. Schaber and L. A. Soderblom, U.S. Geological Survey, Flagstaff, AZ 86001.

mapped is representative of the rest of Venus, then the planet-wide population should be about 900. In this paper we describe the general features of these craters and focus on two significant aspects: (i) the considerable effect of the atmosphere on crater and ejecta morphology and (ii) the implications of the distribution and appearance of the craters for the volcanic and tectonic resurfacing history of Venus.

Crater morphologies and physical properties. The Venera 15–16 radar missions surveyed 115×10^6 km^2 north of 30° latitude. In all, 146 circular features greater than 8 km in diameter of probable impact origin were identified (*1*). Because of its greater resolution, Magellan data expands and clarifies interpretations of crater observations based on Venera images as well as on those images acquired by Earth-based radar facilities (*2–6*).

Impact craters on Venus larger than about 15 km in diameter are similar to those observed on other planetary bodies; they are typically circular and exhibit some or all of the features typical of complex craters (*7*). Such structures result from the potential energy associated with the transient crater cavity, either by direct gravitational collapse (creating terraced walls and flat floors) or possibly by gravity-driven wave phenomena (creating central peaks and peak rings) (*8*). These morphologies are typified by the 48-km-diameter complex crater Danilova (*9*), which exhibits a multiple central peak structure (Fig. 1). As was observed in the Venera 15–16 data (*1, 10*), there is general progression (Fig. 2) with increasing crater diameter from (i) no central structure to (ii) central peak, then to (iii) multipeak or peak ring (Fig. 3).

Of the larger craters, a particularly interesting example is the 105-km-diameter structure Cleopatra Patera, discovered in early Arecibo images (*3*). Cleopatra sits high on Maxwell Montes, and from Venera 15–16 data it was not clear whether this feature was an impact crater or a volcanic caldera (*1, 10–14*). Magellan images reveal that Cleopatra is an impact structure with a peak ring; the primary evidence is the presence of a partially preserved hummocky ejecta facies (Fig. 4). Cleopatra Patera is superimposed on the faults of Maxwell Montes and appears tectonically undeformed; these relations suggest that Cleopatra is very young. Alternatively, Maxwell Montes has been tectonically inactive for a long period; because of the large topographic gradients associated with Maxwell, this notion would require a reassessment of our understanding of venusian lithospheric rheology or temperature structure, or both.

Cleopatra is also interesting because of the large amount of material that appears to have flowed out from the crater floor. A steep-walled, sinuous channel a few kilometers wide breaches the hummocky terrain surrounding the inner crater rim and trends north to northeast across the upper crater floor and passes through a deep breach in the hummocky rim of the outer crater (Fig. 4). The channel continues down the northeastern flank of the outer crater rim, where it appears to be the source of plains deposits filling structural troughs or valleys in Fortuna Tessera immediately east of the base of Maxwell Montes. The existence of the breach in the rim of the outer crater and the plains deposits to the east were recognized from Venera 15–16 images (*12*), and it was suggested that the plains may have originated as volcanic lava flows from the channel breach in Cleopatra's outer rim. Basilevsky and Ivanov (*13*), who championed an impact origin for Cleopatra, suggested that the breach might possibly have been a conduit for post-impact drainage of shock melt from the crater floor.

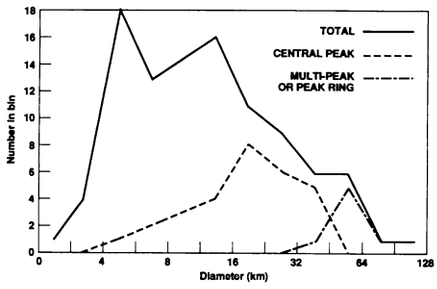

Fig. 2. Frequency distribution of craters with central peaks and with multiple peaks or peak rings. Data are from an analyzed subset of the 135 craters observed.

Most craters smaller than 15 km have some attributes of complex craters, but about half of them are classified as irregular, with noncircular rims and multiple, hummocky floors (Fig. 5). This is interpreted to be the consequence of breakup and dispersion of incoming meteoroids by the dense atmosphere with the near simultaneous impact of the closely grouped fragments. Some of these craters display clear evidence for distinct, overlapping impacts (for example, Fig. 5A). "Crater clusters" contain two or more separate craters that are commonly in rim contact. We attribute them to impacts by fragmented meteoroids dispersed into trajectories that result in separate craters (Figs. 6 and 7). Except for the smallest members of some crater clusters (Fig. 7), no primary craters have been observed that are smaller than 3 km in diameter.

The conditions under which overlapping

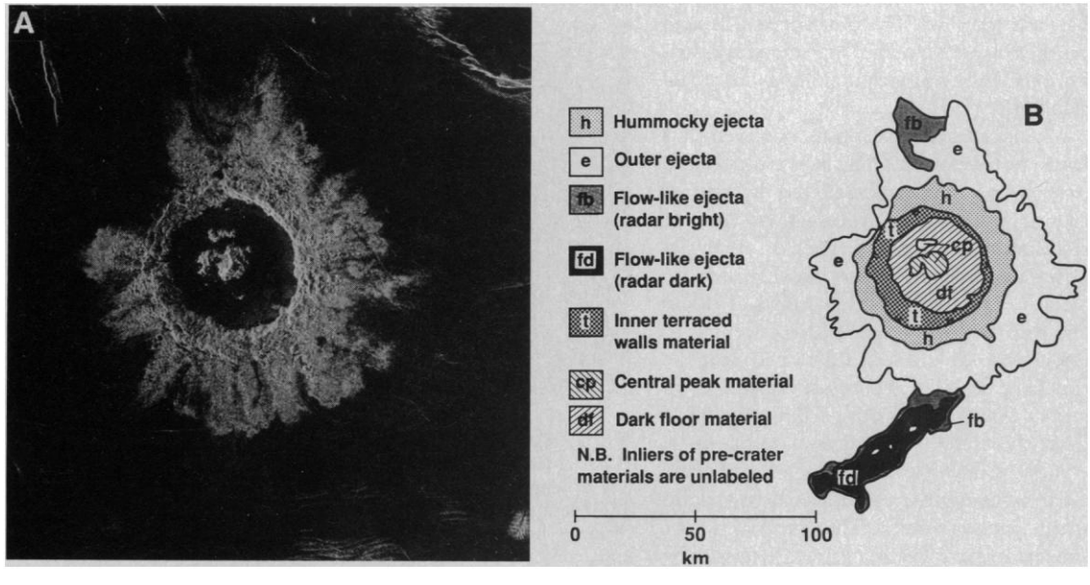

Fig. 1. (**A**) Impact crater Danilova (*9*), 48-km diameter, located at −26.4° latitude, 337.2° longitude (Photo MRPS 35420). (**B**) Geological sketch map.

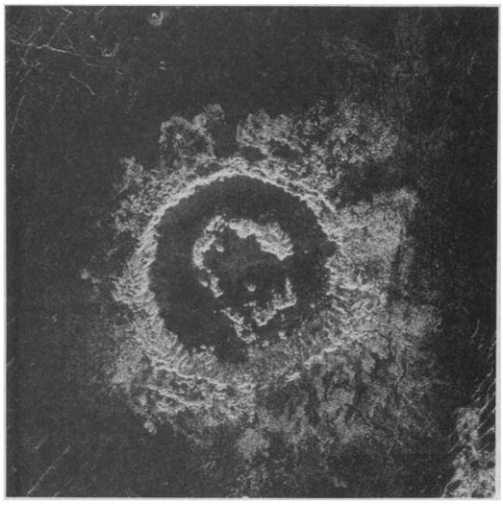

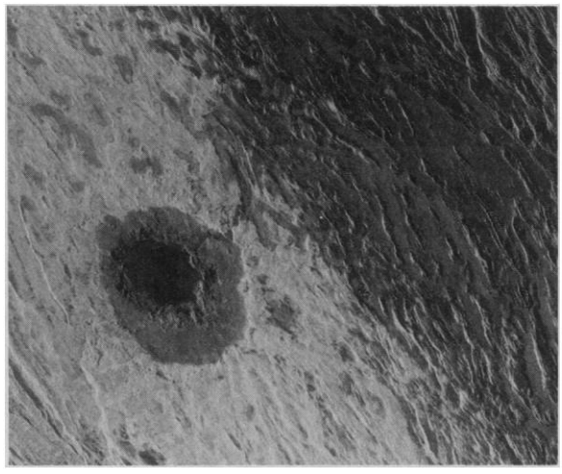

Fig. 3 (**left**). Crater Barton (*9*), 50-km diameter, located at 27.4° latitude, 337.5° longitude, displaying peak-ring structure. North is to left (Photo MRPS 34779).
Fig. 4 (**right**). The 105-km-diameter crater Cleopatra, located at 65.9° latitude, 7.0° longitude and interpreted to be of impact origin (Photo MRPS 35331).

craters and crater clusters will form on Venus can be predicted from theoretical calculations (*8, 15–17*). For an assumed entry angle, meteoroid crushing strength, and Venus model atmosphere, the morphology of the resulting crater form can be predicted as a function of the initial mass and velocity of the meteoroid entering the atmosphere. Meteoroids will either (i) remain coherent; (ii) break up and form, depending on the amount of dispersion, single craters, overlapping craters, or nonoverlapping crater clusters; or (iii) burn up. Calculations for Venus predict that overlapping craters should form in the size range 1 to 10 km (*8*), in reasonable agreement with Magellan observations. Qualitatively, it is expected that most meteoroids entering the atmosphere are crushed by the differential pressure regime encountered, but the amount of dispersion of individual fragments decreases as the initial meteoroid radius increases (*17*). Thus, large meteoroids form only a single crater even though the incoming projectile has been crushed. The exact details depend on the impact velocities and the size distribution of the fragments, among other factors (*18*).

Most crater ejecta deposits observed thus far do not appear, at Magellan resolution, to have been significantly altered by surface erosion, weathering processes, or volcanic resurfacing. Two major types of ejecta deposits are observed around impact craters on Venus. Hummocky ejecta consists of ridges and furrows that are generally concentric to the crater rim and best developed near the rim (Fig. 1). The hummocky ejecta commonly extends from 0.5 to 0.8 crater radii from the crater rim and is thought to be composed mostly of blocks larger than many radar wavelengths, as evidenced by bright, quasi-specular returns. This material is considered to have been emplaced ballistically.

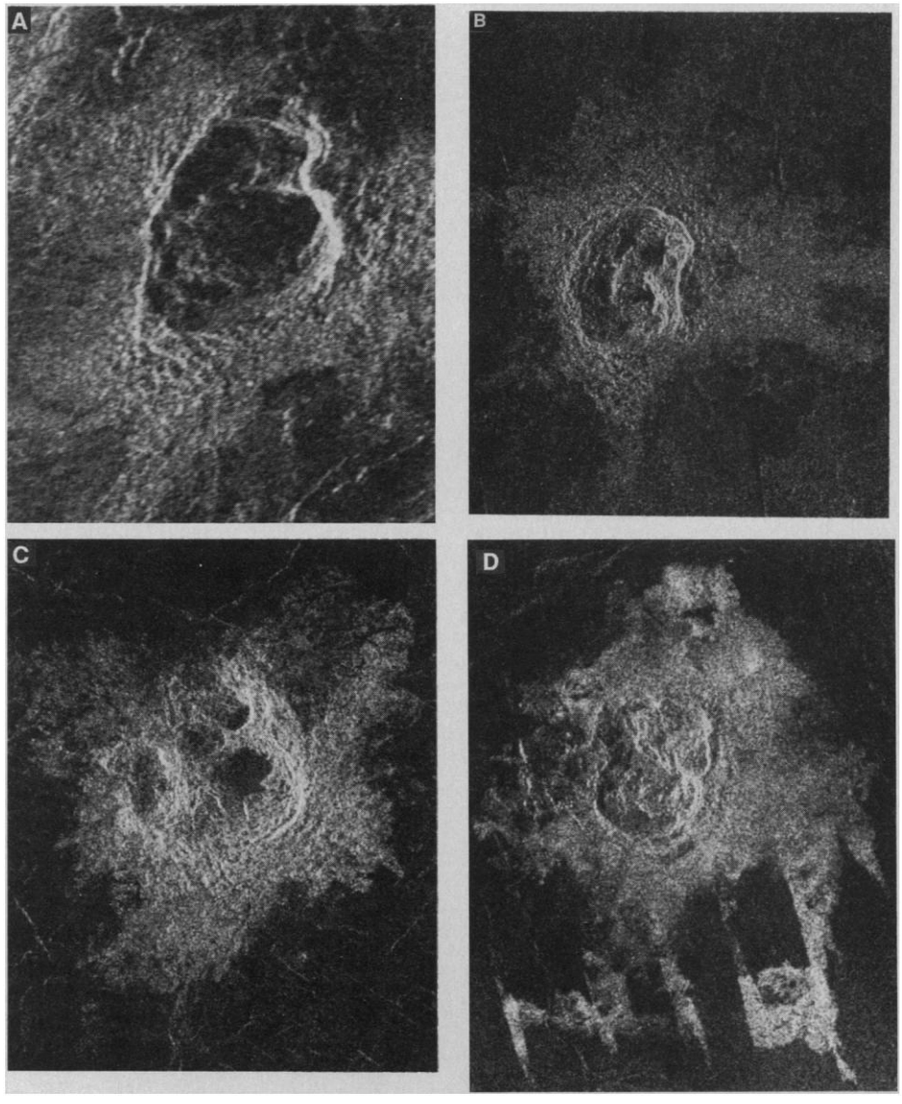

Fig. 5. (**A**) Crater of approximately 11-km mean diameter located at −51.7° latitude, 348.3° longitude (Photo MRPS 33959). (**B**) Crater of approximately 12-km mean diameter located at −21.4° latitude, 335.2° longitude (Photo MRPS 33918). (**C**) Crater of approximately 14-km mean diameter located at 25.6° latitude, 336.0° longitude (Photo MRPS 33958). (**D**) Crater of approximately 9-km mean diameter located at 16.4° latitude, 352.1° longitude. Ejecta distribution on south side of crater is apparently related to graben structures (Photo MRPS 34428).

Surrounding the hummocky ejecta is a generally smoother (not containing large blocks) outer-ejecta facies (*19*). Both facies are typically brighter in the radar images (have higher radar backscatter cross sections, σ_0) than the surrounding plains on which they are emplaced. The distal edge of the outer ejecta of complex craters on Venus is lobate to slightly pointed, commonly with a petal-like appearance (Figs. 1 and 8), suggesting emplacement by flow. The hummocky ejecta appears in some craters to extend radially for some distance along the axes of major lobes of the outer ejecta (Fig. 1). The contact between the two facies is typically well defined for the larger craters but the contact ranges from moderately sharp to quite indistinct around small irregular craters. The outer ejecta of this latter group is commonly irregular, discontinuous, and lacks the lobateness of the larger, complex craters (Fig. 5).

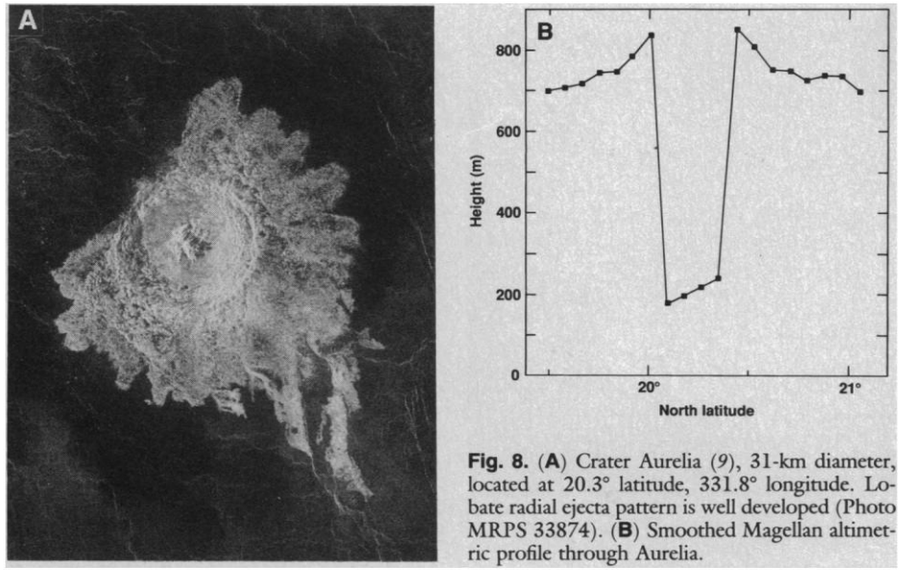

Fig. 8. (**A**) Crater Aurelia (*9*), 31-km diameter, located at 20.3° latitude, 331.8° longitude. Lobate radial ejecta pattern is well developed (Photo MRPS 33874). (**B**) Smoothed Magellan altimetric profile through Aurelia.

Fig. 6. Crater cluster at −30.1° latitude, 345.5° longitude. Mean radius of largest crater is about 13 km. North is to left (Photo MRPS 34798).

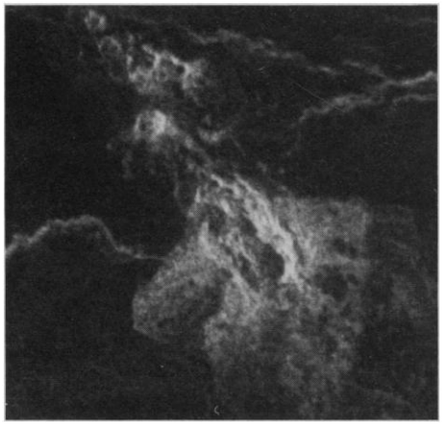

Fig. 7. Crater cluster at 9.3° latitude, 357.8° longitude. Long dimension of largest feature is approximately 11 km (Photo MRPS 34618).

For craters larger than 15 km, the outer ejecta deposits extend outward to a maximum distance of about 2.5 crater radii (Fig. 9). Our initial determination of the average extent of this ejecta is between 50 and 70% of the maximum ejecta distance, as measured from the crater rim (excluding missing sectors; see below), or between 1.75 and 2 radii. Our estimate for ballistic emplacement, on the basis of a gravity-scaling relation derived for atmosphere-free planets, is 1.4 radii (*20*). For Venus, this result would be an upper bound if the only atmospheric effect is that of simple aerodynamic drag on the ejected material. Thus, the radial extent of the outer ejecta significantly exceeds that predicted for simple ballistic emplacement, and other processes must influence the distribution of ejecta.

Atmospheric interactions with ejecta may initiate conditions leading to nonballistic features, specifically the super-ballistic distances and lobate nature of the outer ejecta deposits. The hummocky ejecta, while ballistically emplaced, may undergo continued outward flow due to entrained atmosphere. The outer ejecta deposits may reflect run-out of finer fractions (meter-scale) suspended in turbulent winds created in the lee of a moving ejecta curtain (*21*).

Outer ejecta is not always distributed symmetrically. There are distinctive missing sectors, and the ejecta commonly has a bilateral symmetry or butterfly pattern (Figs. 7 and 10 to 13). This pattern is expected for oblique impacts (*22*), with the major missing sector in the uprange direction; this phenomenon may extend to near-vertical incidence in the presence of an atmosphere because of uprange blockage due to wake interaction and the effects of aerodynamic drag on the ejecta curtain (*23*). In one crater cluster (Fig. 7), the missing ejecta sector lies in the direction of the smaller craters in the cluster, which themselves are expected to be uprange from the largest impact (*16*).

Secondary craters are most recognizable beyond the outer ejecta of craters that appear to have formed by oblique impact (Figs. 10 and 11). In such cases, the secondary craters are more abundant on the downrange side of the primary crater.

A number of craters possess commonly nonradial, flow-like ejecta indicative of flow of a low-viscosity material. Typically these flows extend up to two crater diameters from either beneath or within the crater's hummocky and outer ejecta deposits (Figs. 1, 8, 12, and 14). In some cases (Fig. 1), the ejecta was fluid enough to flow around obstacles such as low volcanic shields; "bathtub rings" of roughened, radar-bright (high σ_0) material left around the obstacles and

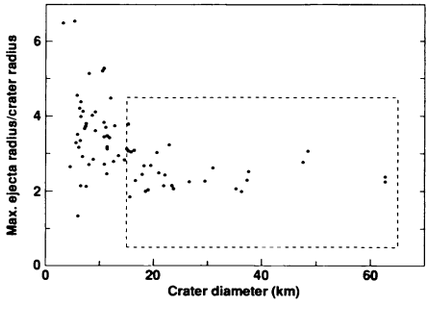

Fig. 9. Ratio of maximum radial distance of outer ejecta to crater radius plotted against crater diameter. Data is from an analyzed subset of the 135 craters observed. Box encloses data points for 30 craters larger than 15-km diameter, for which the mean value was calculated.

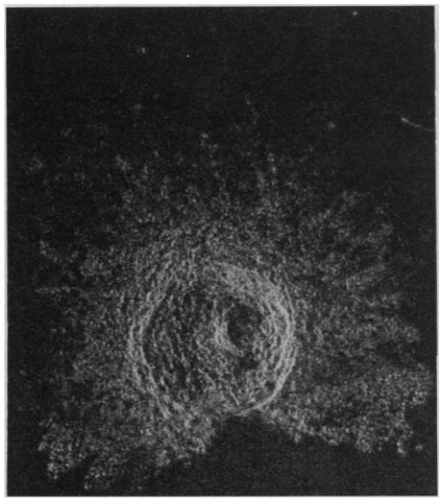

Fig. 10. Crater of approximately 13-km diameter located at 6.0° latitude, 331.9° longitude. Ejecta is missing to the south of crater and secondary craters are concentrated to the north (Photo MRPS 33838).

along the flow edges, as is common for mudflows or debris flows. The presence of these rugged boundaries indicates that the flows must have been energetic. Their thickness can be crudely determined from the heights of volcanic inliers. The shields rise ~100 m or less from the surrounding plains, and because these features are still evident within the flows, the flow thicknesses must be on the order of meters. In addition, because the bathtub rings do not rise high on the flank of the shields, the flow thicknesses during emplacement must have been similar to their present-day values; this relation indicates that the flow behaved as an effective low-viscosity fluid.

The flow-like ejecta has several forms (for example, uniformly radar bright, or bright just along the boundaries), and multiple origins are possible. We consider two models for itsgenesis. The first is an extension of the concept used to explain the lobate nature of some of the distal ends of the outer ejecta facies (*21*). The flow-like ejecta could be the more distal runout of much finer ejecta related to the enhanced thermal turbulence that results from impact-generated melt and vapor. This hot, turbulent flow may be emplaced before the arrival of ballistic ejecta and atmospherically entrained ejecta flows (*23*).

The second model is that the flow-like ejecta is impact melt. In this model, the material is interpreted to flow from shock-melt pools on and within the outer ejecta, and from impact-related fractures extending well below the transient cavity of the crater. Evidence for shock melt pools and flows associated with impact craters was first discovered on the moon with Lunar Orbiter pictures of craters such as Tycho and Aristarchus (*24*). The amount of impact melt generated on Venus and Earth should be larger than on the moon for the same size crater because of the larger gravitational acceleration g and impact velocity v. Internal temperature differences between Earth and Venus probably have a second-order influence (*25*). For a given mass and velocity of the impacting body, larger gravity leads to a reduction in the excavated crater volume but has no effect on melt generation; thus, the melt fraction in the ejecta increases. Scaling relations show that for a given crater size, the volume of impact melt is proportional to $g^{0.533}$ (*26*). The amount of melt depends on impact velocity in an approximately linear fashion (*27*). Gravity and velocity effects taken together predict that, for the same size crater, up to five times as much impact melt should be generated for a Venusian crater as compared to a lunar crater.

Large areas of low radar albedo were observed in early ground-based observations of Venus (*3*), with the radar system aboard the Pioneer Venus orbiter (*28*), and in more recent higher resolution Arecibo images (*29*). It was not until the Magellan data became available, however, that the direct linkage of some of these areas with impact craters was confirmed. Approximately half of the impact craters observed are partially or wholly surrounded by areas with low radar backscatter cross sections (Figs. 1, 3, 7, 8, 11, 12, and 14); we term these areas "dark margins." In most cases, these regions are irregularly shaped and extend up to three or four crater diameters from the crater center; in a few cases, the dark areas are much more extensive. The contact between the dark area and the surrounding brighter terrain varies from well-defined to diffuse.

Additional observations that bear on the origin of dark margins are: (i) occasionally the outer boundary of the dark margins is flow-like or tongue-like (Fig. 12); and (ii) dark-margins material is sometimes observed to have (apparently) removed topography. Northwest of the crater Danilova (Fig. 1A), graben structures are obscured by the Danilova dark margins.

None of the impact craters observed on Lakshmi Planum, the elevated plateau in Ishtar Terra lying between about 57°N and 70°N, have dark margins. The absence of dark margins may be due to some unexplained natural effect that is latitude-dependent, or it may be related to the high elevation of the plateau (3 to 4 km). It may also be an artifact caused by the changing incidence angle of the Magellan radar as the spacecraft moves away from the periapsis latitude of 10°N. At periapsis the incidence angle is 45°, whereas it is close to 25° over Lakshmi Planum. At the 10° to 14° inci-

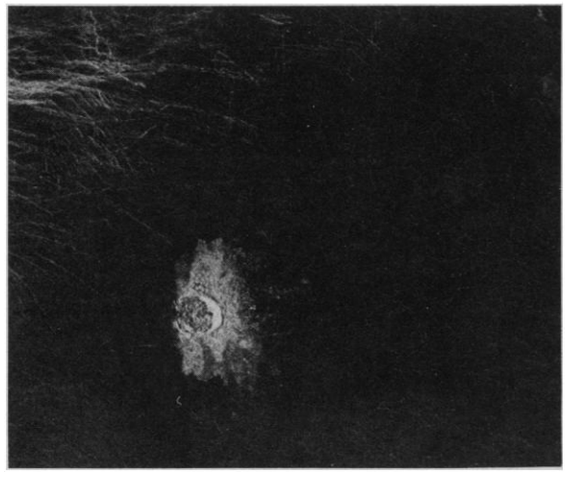

Fig. 11 (**left**). Crater Stephania, approximately 11 km in diameter, located at 51.3° latitude, 333.3° longitude (Photo MRPS 33857).

Fig. 12 (**right**). Crater Jeanne, 19.5 km in diameter, located at 40.0° latitude, 331.4° longitude. Note missing ejecta, out flow material on northwest, and dark margins surrounding crater (Photo MRPS 33856).

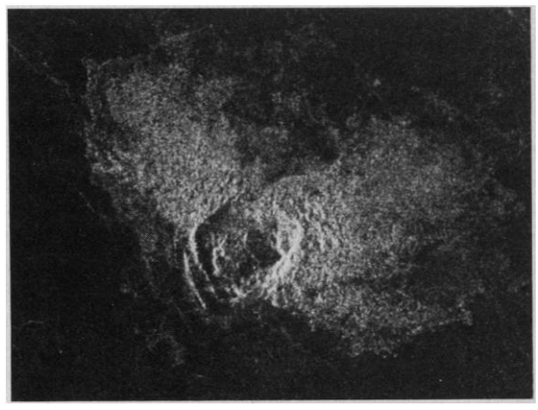

Fig. 13 (left). Crater of approximately 8-km mean diameter located at 11.9° latitude, 352.0° longitude. Butterfly symmetry pattern is especially well developed (Photo MRPS 34427).

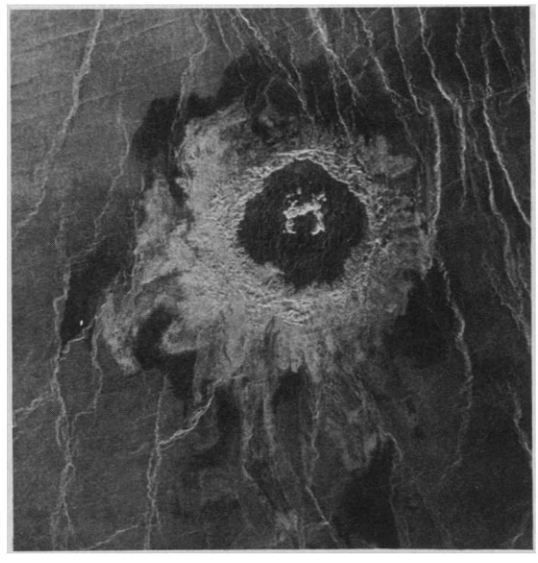

Fig. 14 (right). Crater Cunitz (*9*), 48.5 km in diameter, located at 14.5° latitude, 350.9° longitude, in the faulted plains south of Sif Mons. North is to left (Photo MRPS 34618).

dence angle of the Venera 15–16 radar system, few craters exhibited dark margins (*1*), including some, such as Stephania, which exhibit this feature at the higher Magellan incidence angle. Too few craters have been observed so far to study the relation between incidence angle and the presence of dark margins, but it is possible that many more would exhibit the phenomenon if viewed at high incidence angles.

Because typical dark margins appear to be more visible at the higher incidence angles, it is reasonable to assume that they are smooth areas with little surface roughness of the scale of the radar wavelength. If the dark margins have surface material with a lower Fresnel reflectivity than the surrounding terrain, there should be little dependence on incidence angle. There is little difference in reflectivity and emissivity (*30*) between dark margins and the local terrain for Stephania and for another crater (at 6°N, 332°). This result suggests that the removal of wavelength-size structure from existing terrain may be responsible for the origin of dark margins, and a possible mechanism is the effects of an atmospheric shock or pressure wave produced by the incoming body (*10*). Alternatively, the surface could be blanketed by a deposit of fine material produced either by ablation of the meteoroid during atmospheric transit or during the impact. This hypothesis would be inconsistent with the pristine nature of many of the outer ejecta units unless the dark-margin material is deposited first or is thin enough to not obscure the underlying material.

On Venus, meteoroid-induced shock waves may be capable of damaging the ground surface because peak pressures may reach 10 to 100 MPa, and large dynamic pressures acting up to several minutes may be capable of moving significant volumes of material (*10*). In support of a shock- or pressure-wave origin for the dark margins, there are examples of what we perceive to be dark margins that surround small impact craters or contain no craters at all (Fig. 15). Presumably, meteoroids that would form craters smaller than the observed cutoff diameter of 3 km are not able to penetrate the atmospheric column or they decelerate to velocities insufficient to form impact craters (*1, 8, 10, 15*). However, the accompanying shock or pressure wave may still have sufficient energy to deform the surface, in effect creating dark margins. We estimate that the energy required to create craterless dark margins by pulverizing rock is approximately $E_r \approx \pi \times 10^{15}$ J (*31*). The amount of energy deposited by a meteoroid in the atmosphere is given by $E_a \approx \pi \rho_a v^2 r_m^2 L_t$, where ρ_a is atmospheric density, L_t is the

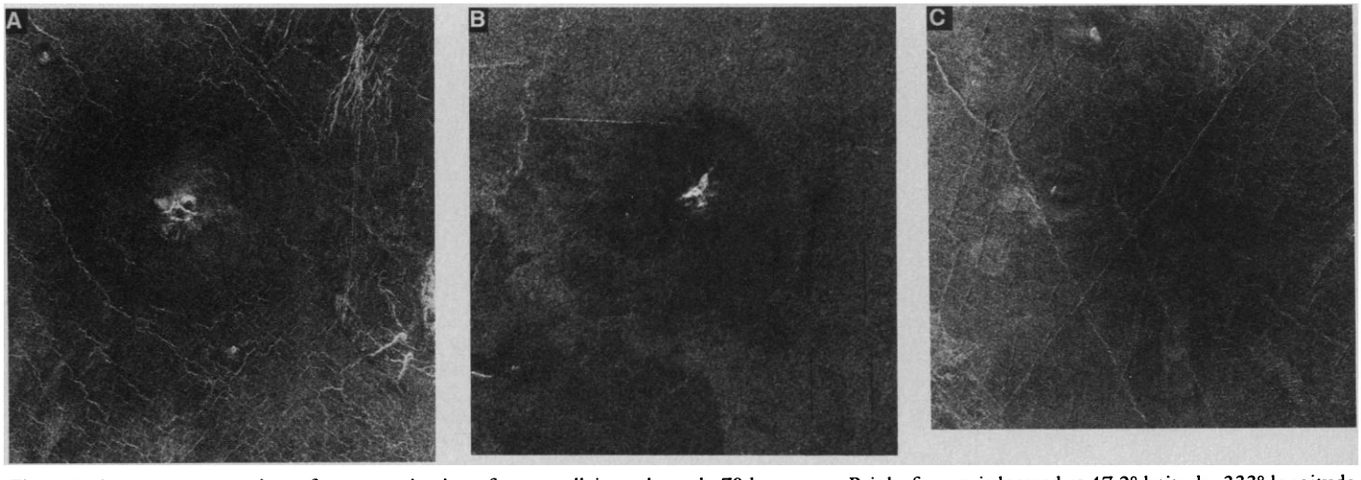

Fig. 15. Apparent progression of crater extinction: from small irregular craters within dark margins to dark margins alone. North is to left in all images. (**A**) Image is approximately 75 km across. Crater is located at −20.7° latitude, 338.6° longitude (Photo MRPS 33962). (**B**) Image is approximately 70 km across. Bright feature is located at 47.2° latitude, 333° longitude (Photo MRPS 33987). (**C**) Image is approximately 70 km across. Center of image is about −19.6° latitude, 338.8° longitude (Photo MRPS 36838).

trajectory path length, and r_m and v are meteoroid radius and velocity, respectively. A meteoroid (or its crushed equivalent) of 100 m radius (r_m) produces, with allowance for deceleration in the atmosphere, an impact crater near or below the observed cutoff diameter (*1*). Equating the two energies and adopting values (*32*) of 40 kg m^{-3} and 20 km for ρ_a and L_t, respectively, yields a required meteoroid velocity of 350 m s^{-1}. Before it strikes the ground, most of the kinetic energy loss of an incoming hypersonic meteoroid is converted into atmospheric heat. Only at relatively low Mach numbers (the supersonic regime) can significant pressure work be created, and it is assumed that the kinetic energy loss at Mach number less than 3 is available, for the most part, to the shock or pressure wave that will deform the planetary surface (*33*). Because the speed of sound in the Venusian atmosphere is about 500 m s^{-1}, it appears that even with a reduced path length, more than sufficient energy is available in the shock or pressure wave to create dark margins, even when no impact crater is formed.

Perhaps the most intriguing and least understood phenomena associated with impact craters are the large parabolic features such as those associated with the craters Aurelia and Carson (Fig. 16). The radar image of Carson shows alternating dark and slightly lighter bands that curve around the eastern side of the crater (which is not precisely centered) and extend to the northwest and southwest for several hundred kilometers. There are also parabolic bands of low emissivity associated with a number of craters in the equatorial region, which (as with the image of Carson) extend from just to the east of the probable impact crater for several hundred kilometers to the northwest and southwest (*34*). The same signature is present in the reflectivity data, and the bands of low emissivity correspond to bands of high reflectivity. The typical emissivity values for the bands are close to 0.80, whereas the values for the surrounding areas are close to 0.85. It is uncertain whether this contrast is due to differences in the wavelength-sized surface roughness or in the intrinsic reflection properties of the surface material. One possibility is that the surface is mantled by fine material that was thrown high into the atmosphere by the impact and fell out as it was transported to the west by high altitude winds.

Size and spatial distribution of impact craters. Impact crater morphology, locations, and size-frequency distributions (Fig. 17) can be used to provide constraints on the nature, rate, and timing of venusian resurfacing processes. The cumulative size-frequency distribution of craters commonly obeys a power law reflecting the size distribution of crater-forming asteroids and comets. If all impact craters are preserved on a planetary surface, the crater abundance increases according to the crater formation rate, and the population is in production. If the formation rate is known, the crater abundance can be used to infer the age of the surface since the time that craters were preservable, that is, since the abeyance of crater-removing processes. Alternatively, craters can be removed at some rate by erosion, by burial under sedimentary debris, by volcanism, and by tectonic processes such as intense faulting. If the crater removal rate is fast enough, over the lifetime of the surface craters will be both produced and destroyed. If the rates have been constant for production and removal, then an equilibrium size-frequency distribution will pertain. Then each crater size will have a retention age equal to some characteristic vertical dimension (kilometers), related to destruction of the crater, divided by the vertical removal rate (kilometers per million years). There can be a critical crater diameter below which craters are in equilibrium and above which they are in production. Of course, production and obliteration rates may also vary with time and place, and quantitative models are required to describe the resultant cumulative size-frequency distributions.

Cumulative size-frequency distributions for the 135 identified impact craters (Fig. 17) indicate that: (i) no primary, nonclustered crater smaller than about 3 km across has been observed, despite the fact that Magellan's resolution is considerably less than 1 km, and (ii) for craters smaller than about 25 km, the cumulative curve does not follow a simple power law; there appears to be a deficiency of small craters. The absence of craters at smaller sizes is evident by extrapolating a power-law curve matched to the cumulative distribution for craters larger than 25 km (Fig. 17); a deficiency of about three orders of magnitude is evident at the

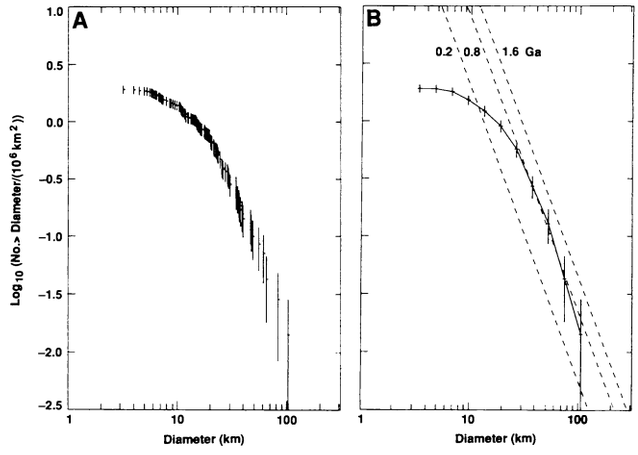

Fig. 16 (left). Crater Carson (*9*), 38-km diameter, located at −24.2° latitude, 344.1° longitude, with parabolic features (Photo FMIDRP 25S345).

Fig. 17 (above). (**A**) Unaveraged (raw) cumulative size-frequency distribution as a function of crater diameter for data gathered over first 277 mapping orbits of Magellan. The information plotted on the vertical axis is the base-10 log of the number of craters (per 10^6 km^2) greater than or equal to the corresponding diameter on the horizontal axis. Error bars are 1-σ limits based on Poisson statistics. (**B**) Same as (A) except that data have been smoothed by binning in $\sqrt{2}$ increments. Also shown are the predictions of a regional-resurfacing model based on the average time to resurface the planet once (see text). Resurfacing times of 0.2, 0.8, and 1.6 Ga are shown.

smallest crater sizes. The absence of small craters was evident in the Venera 15–16 data (*1, 10*) and attributed to atmospheric effects; theoretical models of the passage of meteoroids through the dense Venusian atmosphere are able to match the observed crater deficiency (*1, 8, 10, 15*). In these models, the rollover in the cumulative distribution results mainly from a statistical distribution of atmospheric entry angles, and hence atmospheric path lengths.

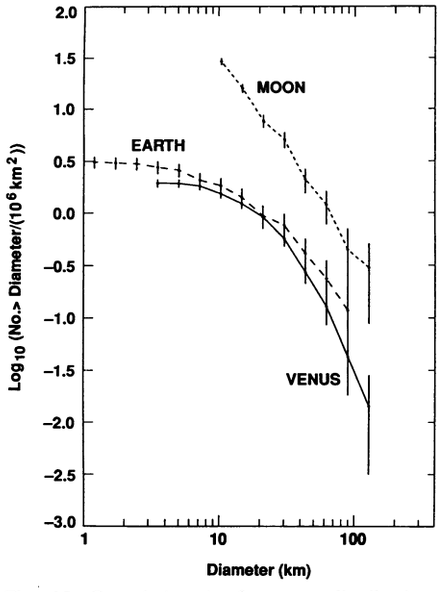

Fig. 18. Cumulative size-frequency distribution comparisons. Magellan-mapped area of Venus (first 277 mapping orbits), Phanerozoic population for the North American and European cratons, and lunar post-mare craters. Error bars are 1-σ limits based on Poisson statistics.

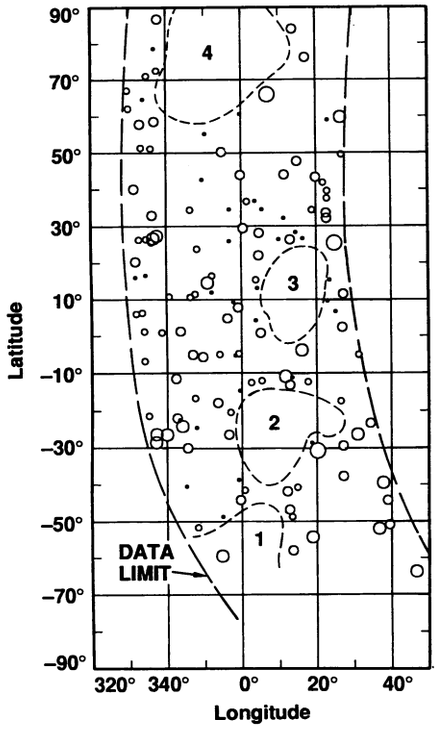

Fig. 19. Areal distribution of craters in first 277 Magellan mapping orbits shown in cylindrical projection. Five different sizes of circles correspond to diameter ranges: <8 km, 8 to 16 km, 16 to 32 km, 32 to 64 km, >64 km. Areas 1, 2, 3, and 4 are in Lavinia Planitia, the area around Alpha Regio, the Sappho Patera region, and an area to the north of Maxwell Montes and to the east of Freyja Montes, respectively, and are examples of regions with no impact craters. Single crater in Lavinia Planitia region is the almost completely flooded crater Alcott (Fig. 20).

The cumulative size-frequency distribution for venusian impact craters (as mapped by Magellan) is essentially identical with the Phanerozoic population of the North American and European cratons (Fig. 18). This is expected if the surfaces counted on the two planets have the same average crater production age or retention age (*35*). The postmare lunar impact craters (Fig. 18) belong to a production population accumulating on surfaces since the end of mare volcanism, about 2.5 to 3 billion years ago (Ga). The relative youthfulness of both the terrestrial and venusian surfaces is evident (*36*).

Impact craters are not uniformly distributed on the surface of Venus (*37, 38, 39*). This is seen in the Magellan data (Fig. 19), where the craters do not appear to have a completely random distribution. Particularly apparent are regions that do not have any impact craters at all.

There could, of course, be large regions devoid of craters in a spatially random distribution. The hypothesis that the observed areal distribution of craters is actually random can readily be tested in the Sappho region (Region 3, Fig. 19). The area around Sappho that is devoid of impact craters is approximately 5×10^6 km^2. We considered 135 (the total number of impact craters observed) independent Bernoulli trials for impact. A success occurs when a crater is formed in Sappho and the probability of success for a spatially random process must be the ratio of the Sappho area to total area surveyed, or 1/14. The resulting probability distribution is binomial, $b(x,135,1/14)$, with $\mu = 9.6$ and $\sigma = 3.0$. This meets the criterion, $\mu \geq 3\sigma$, that ensures the sampling area is large enough to have at least 1 crater (*38*). The probability of observing no craters at Sappho under a random spatial distribution is 4.5×10^{-5} $[b(0,135,1/14)]$. Thus it is highly unlikely that the event of no craters in Sappho can occur randomly. However, this does not reject the hypothesis that the null occurrence of craters can belong to a random process because the Sappho area is part of a larger sampling population. If this experiment is repeated a sufficient number of times (that is, other 5 million square kilometer areas are examined), the probability that at least one such area will be found with no craters will approach unity. The maximum number of experiments possible is 92, the surface area of the planet divided by 5×10^6. The expected number of 5 million square kilometer areas with no craters is approximately $92 \times b(0,135,1/14) = 0.004$ (*40*). Therefore, if Venus truly has a spatially random distribution of impact craters, the probability of finding a region the size of the Sappho area with no craters is essentially nil.

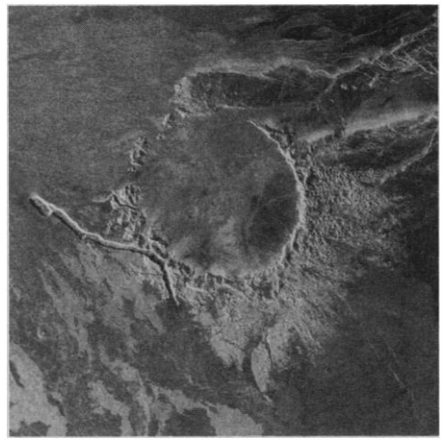

Fig. 20. Crater Alcott (*9*), 63 km in diameter, located at −59.5° latitude, 354.7° longitude, which has been extensively flooded by lava (Photo MRPS 34482).

We conclude that those areas on Venus with few or no impact craters must have young surfaces undergoing rapid resurfacing. At Sappho, volcanism is probably playing a major role in resurfacing (*41*); elsewhere, tectonic processes may also be important.

Early altimetric results (Fig. 8B) show that crater depths are consistent with those found from Venera 15–16 data. With the latter data set, it was shown (*42*) that viscous relaxation does not appear to be an important process for modifying craters on Venus. To first order, the impact craters observed thus far also do not appear to have been significantly modified by surficial processes (*34*). Ejecta deposits consistently maintain the rough topography associated with emplacement; dark margins are also generally preserved, although parabolic features occur on only a few craters (*34*). Several ejecta deposits appear to be embayed by plains materials. In only a few cases is there unambiguous evidence that ejecta has been significantly flooded by lava (Fig. 20), and there are only a few craters that have been significantly modified by volcanism and tectonism in general, that is, modified to the extent that ejecta, rims, terraces, or central peaks have

been removed. These observations suggest that in most areas the rates of weathering, erosion, and burial are incapable of removing craters over the lifetime of the crater population seen in the data. Areas completely devoid of craters must be an exception to this general conclusion.

Four hypotheses are consistent with some or all of these observations. The first is that resurfacing on Venus may have been high up to some point in the past, and all impact craters were removed. Then, the rate declined and craters were preserved, with some infilling by volcanism. In this case, a production size-frequency population should be observed, and a match to the cumulative size-frequency distribution (Fig. 17) for craters larger than 25 km yields a surface age of about 0.4 Ga. For craters larger than 25-km diameter to be in production on, say, a 0.4-Ga surface, the vertical resurfacing rate must be less than about 0.8 km per billion years. This hypothesis is attractive in consideration of the pristine nature of almost all of the impact craters; if correct, it implies that the rate of volcanism has been quite low over the last several hundred million years. In this example, the rate of magma production on Venus would be less than about 20% of the terrestrial rate of 20 km^3 yr^{-1} (*43*), provided that the proportion of magmas intruded into the crust and not erupted is the same as on Earth.

The second hypothesis is that the rate of resurfacing is high and the observed distribution of craters reflects a recent period of enhanced cratering. Testing between these first two alternatives is difficult in the absence of independent age information. Both hypotheses can be criticized on the basis that there are areas on the planet that are obviously not in crater production (Fig. 19).

A surface in equilibrium between crater production and crater obliteration is a third possibility. This hypothesis was considered on the basis of the Venera data, and the maximum resurfacing rate estimated was between 2 and 9 km per billion years, corresponding to retention ages of 280 to 70 Ma (*44*). This possibility is unlikely because in an equilibrium population, a full spectrum of crater degradation states is expected, which is not what is observed thus far.

The fourth hypothesis considers that cratering occurs randomly in space and time, whereas resurfacing does not (*45*). In this case, craters are preserved in relatively pristine form in tectonically and volcanically quiescent regions. Areas of recent volcanism and tectonism have completely removed craters because resurfacing rates have been high. This hypothesis appears to account for the seemingly contradictory observations that: (i) few impact craters are found to be in the process of removal by resurfacing, yet (ii) there are areas of the planet where no impact craters are seen (Fig. 19), and thus there must be processes removing craters on a regional basis.

This hypothesis implies that a production interpretation, if valid, can only represent an average age for the planet and has no meaning on a regional basis. A simple, end-member model for this hypothesis is one of "regional resurfacing." This approach must be only an approximation because the model is binary: either craters are pristine, or they are completely removed; there are no craters in the process of being removed. With this assumption, the cumulative size-frequency distribution, Σ_r, is given by (*46*) $\Sigma_r = \frac{1}{2}(R_p/f_r)D^{-\alpha}$, where R_p is the present cratering rate (*47*), D is crater diameter, f_r is the fraction of the planet resurfaced in one year, and α is the power-law exponent that determines size distribution. The reciprocal of f_r is T_r, the average time to resurface the planet once. In Fig. 17B, Σ_r values are plotted for T_r values of 0.2, 0.8, and 1.6 Ga. The portion of the curve unaffected by the atmosphere ($D \geq 25$ km) is well matched by $T_r = 0.8$ Ga. In this model, there is no one unique age of the entire surface; surface ages span the range from 0 to 800 million years ago, and Sappho, for example, is representative of one of the youngest regions on the planet. We consider this to be the most realistic interpretation of the crater data, in terms of both the cumulative statistics and the appearance of individual craters.

Thus, impact craters provide a means to decipher the spatial and temporal aspects of the recent volcanic history of Venus, and such results can be related to tectonic, topographic, and gravity data to help understand the mechanism and rate by which Venus loses its internal heat.

On the basis of the 15% of the planet that has been surveyed, it is reasonable to conclude from the areal distribution of impact craters, particularly the occurrence of regions devoid of such features, that Venus today is a geologically active planet.

REFERENCES AND NOTES

1. A. T. Basilevsky *et al.*, *J. Geophys. Res.* **92**, 12869 (1987).
2. H. C. Rumsey *et al.*, *Icarus* **23**, 1 (1974); R. M. Goldstein, R. R. Green, H. C. Rumsey, *J. Geophys. Res.* **81**, 4807 (1976); R. S. Saunders and M. C. Malin, *Geol. Rom.* **15**, 507 (1976).
3. D. B. Campbell and B. A. Burns, *J. Geophys. Res.* **85**, 8271 (1980).
4. B. A. Burns and D. B. Campbell, *ibid.* **90**, 3037 (1985).
5. D. B. Campbell, N. J. S. Stacey, A. A. Hine, *Geophys. Res. Lett.* **17**, 1389 (1990).
6. R. E. Arvidson *et al.*, *Proc. Lunar Planet. Sci. Conf.* **20**, 557 (1990).
7. E. M. Shoemaker, in *Physics and Astronomy of the Moon,* E. Kopal, Ed. (Academic Press, London, 1962), pp. 283–359; W. L. Quaide, D. E. Gault, R. A. Schmidt, *Ann. N.Y. Acad. Sci.* **123**, 563 (1965); M. R. Dence, *ibid.*, p. 941.
8. H. J. Melosh, *Impact Cratering, A Geologic Process* (Oxford University Press, New York, 1989).
9. Provisional name.
10. B. A. Ivanov, A. T. Basilevsky, V. P. Kryuchkov, I. M. Chernaya, *Proc. 16th Lunar Planet. Sci. Conf., Part 2, J. Geophys. Res.* **91**, D413 (1986).
11. V. L. Barsukov *et al.*, *ibid.*, p. D378.
12. G. G. Schaber, R. C. Kozak, H. Masursky, *Geophys. Res. Lett.* **14**, 41 (1987).
13. A. T. Basilevsky and B. A. Ivanov, *ibid.* **17**, 175 (1990).
14. A. R. Peterfreund, J. W. Head, R. A. F. Grieve, *Lunar Planet. Sci.* **XV**, 641 (1984).
15. M. E. Tauber and D. B. Kirk, *Icarus* **28**, 351 (1976).
16. Q. R. Passey and H. J. Melosh, *ibid.* **42**, 211 (1980).
17. H. J. Melosh, *Proc. Lunar Planet. Sci. Conf.* **12A**, 29 (1981).
18. P. H. Schultz and D. E. Gault, *J Geophys. Res.* **90**, 3701 (1985).
19. On other planets, this facies has been called "continuous ejecta." We avoid that term for Venus because in many cases there are annular segments around impact craters that are devoid of this ejecta facies (see text).
20. Ratios of the average ejecta distance to crater radius for craters on the airless bodies moon and Mercury are about R_a(moon) = 2.3 and R_a(Mercury) = 1.8, respectively, for craters of a few tens of kilometers in diameter [D. E. Gault, J. E. Guest, J. E. Murray, J. B. Dzurisin, M. C. Malin, *J. Geophys. Res.* **80**, 2444 (1975)]. The disparity in these ratios has been attributed to differential gravitational effects on the slumping and widening of the initial craters, as scaling relations show that ejecta emplacement itself is invariant to gravity, g (*8*). Empirically, R_a(Mercury)/R_a(moon) = $[g(\text{Mercury})/g(\text{Moon})]^{-0.3}$, and this scaling applied to Venus predicts that R_a(Venus) = 1.4.
21. P. H. Schultz and D. E. Gault, *J. Geophys. Res.* **84**, 7669 (1979); *Geol. Soc. Am. Spec. Pap. 190,* 153 (1982); P. H. Schultz, in preparation; personal communication.
22. D. E. Gault and J. A. Wedekind, in *Proc. Lunar Planet. Sci. Conf.* **9**, 3843 (1978).
23. P. H. Schultz, personal communication.
24. E. M. Shoemaker *et al.*, in *Surveyor VII: A Preliminary Report* (NASA SP-173, National Aeronautics and Space Administration, Washington, DC, 1968), p. 13.
25. A. M. Vickery and H. J. Melosh, *Lunar Planet Sci.* **XXII**, 1443 (1991).
26. J. D. O'Keefe and T. J. Ahrens, in *Proc. Lunar Sci. Conf.* **8**, 3357 (1977).
27. R. A. F. Grieve and M. J. Cintala, *Proc. Lunar Planet. Sci. Conf.* **12B**, 1607 (1981).
28. D. A. Senske, thesis, Brown University, Providence, RI (1989).
29. D. B. Campbell *et al.*, *Science* **246**, 373 (1989).
30. See G. H. Pettingill *et al.* [*ibid.* **252**, 260 (1991)] and G. L. Tyler (*ibid.*, p. 265), for a description of these data sets.
31. A stress value, σ, of 10 kbar (1000 MPa) is chosen for rock crushing; this is about ten times as large as the fracture stress indicated by dynamic loading tests [D. E. Grady and M. E. Kipp, in *Fracture Mechanics of Rock* (Academic Press, London, 1987), p. 429]. The dark-margins hypothesis requires that fracturing produces particle sizes on the order of centimeters (fraction of radar wavelength). This can be provided by the high strain rate inherent in impulsive loading by the shock or pressure wave. The energy consumed during deformation is $E_r = (1/2E)\sigma^2 V$, where E is Young's modulus, and V is volume. The value of E used here is 5×10^{10} Pa. The comminuted material must be able to migrate sufficiently in response to the incoming disturbance to form flow features and to mask the radar returns from specular facets of topography. The minimum depth requirement for shock- or pressure-wave disturbance must be at least several radar wavelengths and perhaps as much as 1 m. Typical craterless dark margins are about 20 km in diameter, giving a volume estimate of $\pi \times 10^8$ m^3. This leads to an energy requirement for deformation of $\pi \times 10^{15}$ J.
32. We use 20 km as a characteristic scale height in the venusian atmosphere (density is 30% of surface value); the average atmospheric density in this inter-

val is 40 kg m^{-3} (*10*).
33. R. P. Turco *et al.*, *Icarus* **50**, 1 (1982).
34. See R. E. Arvidson *et al.* [*Science* **252**, 270 (1991)] for a more extensive description.
35. Retention ages for 20-km-sized craters on the North American and European cratons depend on erosion rate and lithology and vary from 34 to 630 Ma. Most craters larger than 20 km are recognizable to ages of 120 Ma, which gives a lower bound on retention age [R. A. F. Grieve], *Proc. Lunar Planet. Sci. Conf., Part 2, J. Geophys. Res.* **89**, B403 (1984).
36. The terrestrial data are from R. A. F. Grieve and M. R. Dence [*Icarus* **38**, 230 (1979)]; the lunar data are from R. Strom (personal communication).
37. G. A. Burba, *Lunar Planet. Sci.* **XX**, 123 (1989).
38. J. J. Plaut and R. E. Arvidson, *J. Geophys. Res.* **93**, 15,339 (1988).
39. G. G. Schaber, *U.S. Geol. Surv. Open-File Rep. 90-468* (1990).
40. W. Feller, *An Introduction to Probability Theory and Its Applications* (Wiley, New York, 1962).
41. Image mosaics for the Sappho region were not available when this paper was prepared, so no geological assessment has been made.
42. R. E. Grimm and S. C. Solomon, *J. Geophys. Res.* **93**, 11,911 (1988).
43. Mean oceanic crustal thickness of 6 km multiplied by plate creation rate of 3 km^2 yr^{-1} [B. Parsons, *Geophys. J. R. Astron. Soc.* **67**, 437 (1981); A. Reymer and G. Schubert, *Tectonics* **3**, 63 (1984)].
44. R. E. Grimm and S. C. Solomon, *Geophys. Res. Lett.* **14**, 538 (1987).
45. R. E. Arvidson *et al.*, *ibid.* **17**, 1385 (1990).
46. This result can be derived as follows: Consider that the resurfacing rate is linear in time and that the time to resurface the planet once is given by T_r. Then there is a complete spectrum of production ages ranging from the present back to T_r, and all ages are equally likely to be found on the planet. For any given age, t, within this spectrum, the total number of craters found on the planet is given by

$$\Sigma_r(D,t) = R_p t D^{-\alpha}\, da$$

where da is the incremental surface area of the planet of production age t. The total number of craters on the planet can then be obtained by integrating over the surface area of the planet. Equivalently, if f_r is the fractional resurfacing rate (fraction of planet resurfaced per unit time), then da is related to incremental time dt by $da = Af_r dt$. Then the total number of craters may also be obtained by integrating over all possible production ages

$$\Sigma_r(D) = D^{-\alpha} \int_0^{T_r} R_p t A f_r dt$$

$$= R_p \frac{T_r^2}{2} A f_r D^{-\alpha}$$

Cumulative size-frequency density is obtained by dividing by planetary surface area, and noting that T_r must be the reciprocal of f_r, we then find that

$$\Sigma_r(D) = \frac{1}{2} \frac{R_p}{f_r} D^{-\alpha}$$

47. Estimates of R_p and α are based on the production rate of craters >20 km in diameter by Venus-crossing asteroids, not including asteroids of cometary origin or active comets (E. M. Shoemaker and C. S. Shoemaker, in *The New Solar System*, J. K. Beatty and A. Chaikin, Eds. (Sky Publishing, Cambridge, MA, 1990), pp. 259–274.
48. This work was supported in part by various Magellan contracts from the Jet Propulsion Laboratory, California Institute of Technology, to the authors' home institutions, and by a grant from NERC to J.E.G. at the University of London Observatory. R.J.P. was also supported by NASA grant NAGW-459 to Southern Methodist University. We would like to thank R.E. Grimm, R. R. Herrick, M. Ravine, P. Schenk, V. L. Sharpton, N. Stacy, and C. Wiles. S. Yewell helped provide the photographic products for this paper. Useful comments on the original manuscript were supplied by H. J. Melosh, and R. A. F. Grieve and P. H. Schultz provided detailed reviews. We gratefully acknowledge the Magellan teams at JPL and Martin Marietta who made all of this possible.

8 January 1991; accepted 18 March 1991

Venus Tectonics: Initial Analysis from Magellan

SEAN C. SOLOMON, JAMES W. HEAD, WILLIAM M. KAULA, DAN MCKENZIE, BARRY PARSONS, ROGER J. PHILLIPS, GERALD SCHUBERT, MANIK TALWANI

Radar imaging and altimetry data from the Magellan mission have revealed a diversity of deformational features at a variety of spatial scales on the Venus surface. The plains record a superposition of different episodes of deformation and volcanism; strain is both areally distributed and concentrated into zones of extension and shortening. The common coherence of strain patterns over hundreds of kilometers implies that many features in the plains reflect a crustal response to mantle dynamic processes. Ridge belts and mountain belts represent successive degrees of lithospheric shortening and crustal thickening; the mountain belts also show widespread evidence for extension and collapse both during and following crustal compression. Venus displays two geometrical patterns of concentrated lithospheric extension: quasi-circular coronae and broad rises with linear rift zones; both are sites of significant volcanism. No long, large-offset strike-slip faults have been observed, although limited local horizontal shear is accommodated across many zones of crustal shortening. In general, tectonic features on Venus are unlike those in Earth's oceanic regions in that strain typically is distributed across broad zones that are one to a few hundred kilometers wide, and separated by stronger and less deformed blocks hundreds of kilometers in width, as in actively deforming continental regions on Earth.

IT HAS BEEN KNOWN FOR MORE THAN A decade that the Venus surface preserves a rich and complex history of deformation of the lithosphere, the layer of long-term strength that constitutes the outer shell of every terrestrial planet. The Pioneer Venus altimeter revealed the presence on Venus of such large-scale tectonic structures as great rift zones and linear mountain belts (*1–3*). Radar images of the surface obtained by the Venera 15–16 orbiters (*4, 5*) and Earth-based radar observatories (*6–10*) have shown a variety of features interpreted to be of tectonic origin. The radar images from Magellan constitute an improvement in resolution by at least an order of magnitude over the best images previously available (*11*). In this paper, we discuss what those images, and their interpretations, are revealing about the styles of lithospheric deformation on Venus, the inferred mechanical properties of the lithosphere, and their implications for the tectonic history of the planet. We restrict the discussion principally to data obtained during the first month of mapping, representing about 15% of the surface of the planet.

S. C. Solomon, Department of Earth, Atmospheric, and Planetary Sciences, Massachusetts Institute of Technology, Cambridge, MA 02139.
J. W. Head, Department of Geological Sciences, Brown University, Providence, RI 02912.
W. M. Kaula and G. Schubert, Department of Earth and Space Sciences, University of California, Los Angeles, CA 90024.
D. McKenzie, Bullard Laboratories, Cambridge University, Cambridge CB3 OEZ, England.
B. Parsons, Department of Earth Sciences, Oxford University, Oxford OX1 3PR, England.
R. J. Phillips, Department of Geological Sciences, Southern Methodist University, Dallas, TX 75275.
M. Talwani, Houston Area Research Center, The Woodlands, TX 77381.

Plains deformation. The plains, which constitute more than 80% of the surface of Venus (*2*), are generally low-relief areas with surface deposits of volcanic origin (*12, 13*). Although a few plains regions viewed by Magellan to date are nearly devoid of tectonic features, most show considerable evidence for deformation in a variety of forms and patterns (*11*) that in some areas are consistent over distances of hundreds of kilometers. Because of the generally limited magnitude of horizontal strain in most plains regions, the sense of strain and its relation to regional topography can be more evident in the plains than in areas of greater relief and more intensive deformation.

One of the regions of more extensively deformed plains is centered near 32°N, 335°E, between Guinevere and Sedna Planitiae. [A global map of named features is in (*11*)]. Throughout an area of about 10,000 km^2, these plains are marked by hundreds of prominent lineations trending approximately NW. In one part of this region (Fig. 1) the lineations are paired normal faults bounding flat-floored depressions spaced 0.5 to 3 km apart. These features are interpreted to be simple graben, the result of limited horizontal stretching of the upper crust in the NE-SW direction. A few bright, irregular depressions trending WNW to E-W appear to consist of coalesced sections of NW-trending graben and may represent a younger episode of more nearly N-S extension.

The plains record a continuing interplay between deformation and volcanism. For example, in another area (Fig. 2) approximately 150 km to the SE of that shown in